

# Soft Matrix: Extracting Inherent Length Scales in Sheared Amorphous Solids

Monoj Adhikari, Smarajit Karmakar, and Vishnu V. Krishnan  
*Tata Institute of Fundamental Research, 36/P, Gopanpally Village,  
Serilingampally Mandal, Ranga Reddy District, Hyderabad, 500046, Telangana, India*

Pinaki Chaudhuri  
*The Institute of Mathematical Sciences, CIT Campus, Taramani, Chennai 600113, India and  
Homi Bhabha National Institute, Anushaktinagar, Mumbai 400094, India*

Nandlal Pingua and Shilditya Sengupta  
*Department of Physics Indian Institute of Technology Roorkee 247667 Uttarakhand, India*

Aparna Sreekumari and Vishwas V. Vasisht  
*Department of Physics, Indian Institute of Technology Palakkad,  
Nila Campus, Kanjikode, Palakkad 678623, Kerala, India*

Amorphous solids yield upon crossing a strain threshold, after an initial elastic response, when subjected to mechanical deformation. The yielding process is characterized by local plastic events leading to non-affine displacements, and their interactions. Despite the lack of long-range structural order, these disordered materials exhibit long-range spatial correlations in the non-affine displacement fields, which stems from the underlying elasticity. Measuring a correlation length scale in deformed amorphous solids, during the plastic process, is a non-trivial challenge, often requiring an ad-hoc definition of localized regions. In this paper, we introduce a novel computational approach called the "soft matrix" that enables systematic analysis of mechanical response of local regions within a disordered solid. In this method, we subject the amorphous solid to a quasistatic shear and allow a local region of interest to relax freely while allowing for elastic relaxation of the background. The dependence of the yield strain upon the size of the probe region naturally reveals the existence of an intrinsic length scale ( $\zeta$ ) that governs the elasto-plastic properties, as observed in four distinct model amorphous solids. This finding demonstrates the universality of this characteristic length scale across a wide range of materials. We investigate the dependence of this length scale on the material's preparation history and find that  $\zeta$  increases with better annealing. Furthermore, the local mechanical properties measured within this framework provide more accurate estimates compared to existing techniques. Our study paves the way for a comprehensive understanding of amorphous solids and facilitates improved characterization and design of these materials.

## I. INTRODUCTION

Amorphous solids are disordered systems which are lacking long-range structural ordering. They encompass a broad range of materials ubiquitous in our daily lives, including colloids, foams, emulsions, granular matter as well as metallic and silicate glasses [1]. When subjected to an external load, such as shear deformation, they display an elastic response at low strain values and yield beyond a threshold strain [1–8]. Unlike the crystalline systems where defects are known to be carriers of plasticity, the physical mechanisms underlying the shear response of an amorphous material still lacks a complete understanding. The last two decades of research in theory and experiments have revealed that the plasticity in amorphous solids occurs through local non-affine displacements or rearrangements resulting in the redistribution of elastic stresses within the system [9–11]. Simulation works on athermal systems performed under quasistatic shearing conditions have shown that the displacement field exhibits a quadrupolar symmetry resembling the Eshelby inclusion model [11–14].

Amorphous materials exhibit structural and dynamical

heterogeneities [15]. In recent years, there has been a growing interest in understanding the possible existence of a characteristic length scale associated with the relaxation process in driven amorphous solids. This interest stems from its impact on various aspects, including shear start-up properties [7, 16–20], yielding mechanisms [21–24], and flow heterogeneities [7, 18, 25–27]. Previously, static correlation lengths have been extracted using non-affine shear deformation protocols for colloidal glasses and supercooled liquids [28–30], which demonstrated that the measured lengthscale is highly dependent on the applied shear deformation and likely describes the structural correlations in the initial configuration. Similar protocols have been employed to extract the correlation length in athermal colloidal suspensions under steady-state flow with finite-rate shearing [31], showing dependence on both shear strain and shear rate. Based on ideas of non-local fluidization, a similar dynamical correlation length has also been predicted and measured [32–34]. However, a comprehensive comparison between the extracted correlation length and other measures of static length scale that do not involve shear deformation protocols, such as the point-to-set length

scale [35], length scales obtained from finite-size scaling of relaxation times [36], or minimum eigenvalues [37], is lacking.

Despite the absence of a clear measure of the characteristic length scale, various approaches have been proposed and utilized to characterize the size of plastic events or the number of particles involved in non-affine rearrangements. These methods include analyzing structural properties (e.g., free volume [38], local ordering [39]) and linear response measures (e.g., elastic moduli [40], soft modes [41]). The frozen matrix method has recently gained widespread use in computing local mechanical properties, including yielding thresholds and viscoelastic properties. Initially proposed for assessing local elastic properties [42], this method involves allowing only the specific "target" local region of interest to relax independent of the background. Under external loading, the entire system undergoes a uniform affine deformation, except that the local region is permitted to relax freely, while the rest of the system is restricted from undergoing non-affine relaxation. By analyzing the stress response in the target region to the applied strain, the local mechanical properties can be determined.

The frozen matrix method has been widely utilized in various studies on amorphous solids [43–49]. However, in all cases, the size of the target region is chosen in an ad-hoc manner, and the background material is not allowed to undergo any relaxation and is made rigid - hence frozen. Although this approach provides reasonable estimates of the local yield stability distribution, it tends to overestimate the local yield stress and elastic modulus significantly due to the presence of a rigid background [43, 44, 46, 48]. This overestimation can have an impact on the predictability of local plastic events and the correlations between them. Additionally, the frozen matrix method does not enable the extraction of the length scale associated with the plastic event.

In this study, we introduce a novel approach called the "Soft matrix method" to investigate the local mechanical properties, as described in the following section. This method builds upon the original proposition of the frozen matrix approach and it actually provides us a route to extract a characteristic length scale  $\zeta$  in various types of amorphous materials, overcoming the limitations imposed by rigid or periodic boundary conditions [50, 51]. We observe that this length scale is influenced by the aging conditions of the material, and we demonstrate that it exhibits scale-free power law behavior when studying larger sub-systems. Consequently, this length scale provides a natural solution to the question of appropriate coarse-graining length, serving two main purposes: (a) enabling accurate computation of local mechanical properties crucial for understanding the yielding phenomenon and providing inputs for mesoscale modeling of amorphous materials and (b) facilitating comparisons between this length scale and other measures of static length scale in disordered systems.

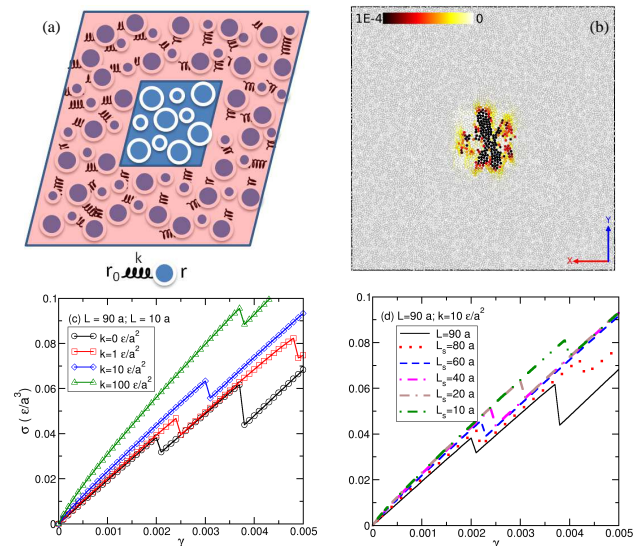


FIG. 1. **Soft Matrix Methodology.** (a) Schematic demonstrating the soft matrix method. The sub-system (central blue box) is subjected to unconstrained relaxation, whereas the background (surrounding pink region) relaxes with a constraint imposed by the spring tether (see text for details). (b.) Snapshot from 2D BMLJ (65:35) simulation illustrating the soft matrix: plastic event is confined to subsystem, while the background is allowed to elastically relax. Here X is the shearing direction, and Y is the gradient direction. (bottom) Variation of stress ( $\sigma$ ) as a function of strain ( $\gamma$ ) for (c) fixed subsystem size ( $L_s = 10a$ ) and varying  $k$  value and (d) fixed  $k$  value ( $k = 10\epsilon/a^2$ ) and varying subsystem size  $L_s$ .

## II. SOFT MATRIX METHOD

In this approach, within a system having linear dimension  $L$ , we choose a local region having size  $L_s$ , whose mechanical properties we plan to measure. The rest of the system from hereon will be referred to as the background. The mechanical response of the solid is probed via the athermal quasi-static shear (AQS) protocol (*see Methods*). The entire system is first subjected to a simple shear deformation of magnitude  $\delta\gamma \approx 10^{-5}$ , and hence an affine displacement is imposed on all particles in the system. Post deformation, the system is subjected to relaxation or energy minimization, and here we introduce an essential improvement over the existing frozen matrix method [43–46] which is key to extracting the heterogeneity length scale  $\zeta$ . Unlike the frozen matrix method, during the energy minimization, the background can relax by affine rearrangements, but no plastic events are permitted in the background. On the other hand, the sub-system is allowed to relax without any constraints. Hence we term the procedure a *soft matrix method*. We implement this partial relaxation of the background by adding an additional spring force of the type  $F_r = -kr$ , before minimization. Here the spring constant  $k$  is a tunable parameter determining the coefficient of restoring force, and  $r$  is the displacement of a background particle

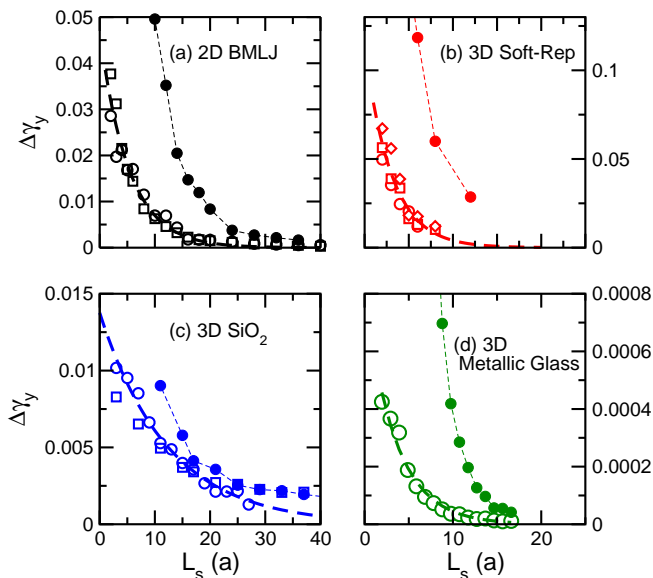


FIG. 2. **Measuring characteristic length scale.** Relative yield strain  $\Delta\gamma_y$  as a function of subsystem size  $L_s$  for four different models: (a) 2D BMLJ (b) 3D Soft-Rep (c) 3D  $\text{SiO}_2$  and (d) 3D Metallic glass. The open symbols are data obtained from the soft matrix method. The opaque symbols are from the frozen matrix method. Different symbols correspond to different system sizes. The thick dashed line is the exponential fit, and the thin dashed line is just a guide to the eye.

from its reference position, taken to be the position after applying the step of affine displacement.

We test out the soft matrix method via extensive numerical simulations using the **2D BMLJ** model and later apply our understanding to study three other model amorphous solids, namely **3D Soft-Rep**, **3D  $\text{SiO}_2$** , and **3D Metallic Glass**. See *Methods* for further details. All the simulations were carried out using LAMMPS molecular dynamics package [52].

In Fig.1, we show (a) schematic and (b) actual simulation configurations for the 2D BMLJ model with  $L = 90a$  and the number of particles  $N = 10000$ . Here  $a$  represent the unit length scale. The background region (pink in Fig.1a)) is subjected to additional restoring force during the relaxation with an appropriate  $k$  value such that (almost) no irreversible plastic motion is observed in the background particles. In Fig.1(b), the colored particles in the sub-system relax with both affine and non-affine displacement and can involve in plastic events. The color bar is based on the magnitude of displacement.

### III. SHEAR STARTUP RESPONSE - FIRST PLASTIC EVENT

In Fig.1(c), we show the load curves (shear stress  $\sigma$  vs. applied strain  $\gamma$ ) for a range of  $k$  values at a fixed subsystem size ( $L_s = 10a$ ) for the 2D BMLJ model. For a

chosen sample, prepared by the standard quench protocol (see *Methods*), we initially perform an AQS simulation of the entire system and obtain the bulk stress-strain curve (load curve), via which we recognise the first local yielding event (referred to herein as the first plastic event) and also identify the spatial location of the event as well as the particles participating in the yielding event (see *Methods*). We construct a sub-box of linear length  $L_s$  around the first plastic event and perform the partial relaxation of the surrounding. The bulk load curve corresponds to  $k = 0$ . In Fig.1(c), we show that with an increase in chosen  $k$  values, the system's shear modulus increases, as clearly observed via an increase in the slope of the stress-strain curve, which implies that the system becomes more and more rigid. Further, with increasing  $k$ , the first plastic event is also delayed and occurs at a higher strain value; thereby the local yield stress value also increases. As  $k \rightarrow \infty$ , we should reach the frozen matrix limit, and that is consistent with our observed trend of larger yield stress and larger strain thresholds with increasing  $k$ .

In the current work, we are primarily interested in determining the heterogeneity length scale  $\zeta$ . Hence, for further analysis, we fix the value of  $k$  by the following two competing requirements: (i)  $k$  should be small enough so that the probe itself does not significantly alter the local mechanical properties of the system, and (ii)  $k$  should be large enough such that (almost) no plasticity occurs in the background system during the stress relaxation. We verify (i) by monitoring the bulk modulus and pressure, which remain unchanged for a range of  $k$  values. For condition (ii), we monitor the displacement in the sub-system and surrounding and find that for appropriate  $k$  values, the background shows no large displacements. (See *SI* for further details).

Having the fixed  $k$ , we now examine the effect of subsystem size  $L_s$  on the load curve, specifically on the yielding strain. In Fig. 1(d) we show load curves for  $k = 10\epsilon/a^2$  for varying  $L_s$ . The solid black line represents the load curve for an unconstrained system which shows a yield strain of  $\gamma_y \approx 0.002$  at the first plastic event. With varying  $L_s$ , the initial linear response does not show much variation, but we observe a systematic change in local yield strain  $\gamma_y$  and local yield stress  $\sigma_y$ . With the increase in  $L_s$ ,  $\gamma_y$  and  $\sigma_y$  decrease. Approaching  $L_s \rightarrow L$ , we recover the unconstrained load curve. We find similar features in the other three model systems that we have studied. In each case, the value of  $k$  was fixed according to the above-prescribed protocol. One can rationalise the increasing yield stress and strain with decreasing  $L_s$  in terms of interface effects, with the background curtailing the motion of particles in the sub-system and hence increasing the barrier height for the first plastic event. However, we find a more interesting observation when we look at the variation of  $\gamma_y$  with  $L_s$ , which we discuss below.

#### IV. A CHARACTERISTIC LENGTH SCALE $\zeta$

In Fig. 2, we show the variation of relative yield strain  $\Delta\gamma_y$  with the sub-system size  $L_s$  for the four different models of amorphous solids. The relative yield strain  $\Delta\gamma_y$  is defined as the deviation of  $\gamma_y$  from the bulk value:  $\Delta\gamma_y = \gamma_y(L_s) - \gamma_y(L)$  where  $\gamma_y(L)$  is the yield strain for the bulk system ( $k = 0$ ). The data shown in Fig. 2 corresponds to poorly aged samples, and we obtain the average  $\Delta\gamma_y$  over multiple initial configurations as well as different system sizes (whenever possible). All four systems show  $\Delta\gamma_y$  decreases exponentially as we increase the size of the probing zone  $L_s$ , suggesting the existence of a characteristic length scale. The exponential fit function  $a_0 \exp(-L_s/\zeta)$  is shown as dashed lines. Here the fit parameter  $a_0$  represents the limiting value of the relative yield strain in the limit of zero sub-system size, and  $\zeta$  is the estimated value of the characteristic heterogeneity length scale intrinsic to each model system. In 2D BMLJ and 3D Soft-rep models, which have short-range interactions, our fit finds  $\zeta \approx 5a$ . Interestingly, this is similar in magnitude to values often assumed in the literature for local rheological measurements in similar models [40, 44, 46], where it is interpreted as the length scale below which Hooke's law for linear continuum elasticity breaks down. For the first time, we have provided the rationality of this choice by directly extracting an intrinsic scale via the proposed soft matrix method. For 3D  $\text{SiO}_2$  and 3D Metallic glass, we find  $\zeta$  to be  $\approx 12a$  and  $\approx 8a$  respectively. The higher values in these models are possibly due to the long-range nature of inter-particle interactions, unlike the Lennard-Jones-type models typically studied. In Fig.2, we also show corresponding data obtained using the frozen method for the purpose of comparison. It is important to note that at small sub-system lengths, the stress shows a significant increase for the frozen matrix method, indicating the influence of how the background relaxation is modeled. This rise is expected to depend on the system size, and in larger system simulations, the impact of the interface will diminish, which is what we observe. Thus, we argue that this approach is not suitable for accurately extracting any characteristic scale which is much less than system size.

#### V. AGE DEPENDENCE OF CHARACTERISTIC LENGTH SCALE, $\zeta$

After extracting the characteristic length scale from the exponential relationship between the local yield strain and the probe window size, we now investigate the influence of the preparation protocol on this length scale.

It is well known that the mechanical response varies dramatically with the increasing age of the amorphous solid samples [2, 20, 53–55]. For example, a poorly aged or annealed sample often shows more homogeneous ductile-like yielding behavior, while a well-aged or ultra-

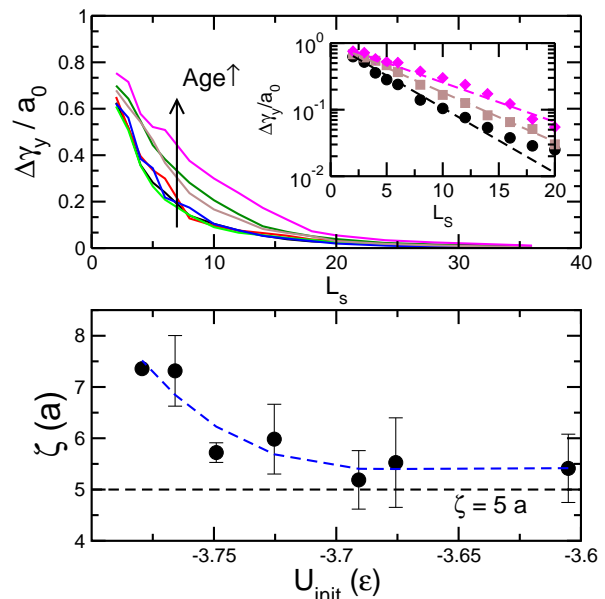


FIG. 3. **Age dependence.** (a) Relative yield strain as a function of subsystem size for different ages of the initial sample (shown for 2D BMLJ). The inset has the same data in log-linear scale, for selected ages. Dashed lines represent fits to exponential functions, from which respective characteristic length  $\zeta$  is extracted. (b) Characteristic length  $\zeta$  as a function of energy of the initial state (i.e. at zero strain),  $U_{\text{init}}$ ; note that  $U_{\text{init}}$  decreases with an increase in age. The dashed line is a guide to the eye.

stable glassy sample exhibit heterogeneous brittle-like yielding via shear banding [20, 21, 56]. Thus it is essential to understand how the characteristic length scale that we obtained using our soft-matrix method depends on the sample age or annealing history, which is presented here for 2D BMLJ glass. We study samples quenched by infinite cooling rate (obtained by energy minimization of configurations generated at different initial temperatures  $T_W$  to instantaneous inherent structures) as well as the ones prepared via finite cooling rate  $\Gamma$  [57]. We then compute the  $\Delta\gamma_y(L_s)$  via the soft matrix method protocol - see Fig. 3 (a) main panel; note that we have scaled the abscissa by the age-dependent fit parameter  $a_0$  for better clarity. We find that  $\Delta\gamma_y$  has a slower decay with  $L_s$ , for increasing age of the system. The exponential nature of  $\Delta\gamma_y(L_s)$  is clearly shown in the inset of Fig. 3 (a), via linear-log scale. Therefore, it is evident that with increasing age, the characteristic length scale increases significantly. The extracted  $\zeta$  as a function of the energy of the sample at zero strain is shown in Fig. 3 (b); lower energy of the initial state indicates higher age of the sample. We see that the value  $\zeta \approx 5a$  occur only for a range of the poorly aged sample, and  $\zeta$  systematically increases with an increase in age. Hence our analysis clearly suggests that any measure of local mechanical properties should consider the  $\zeta$  dependence with age. Further work needs to be done to understand



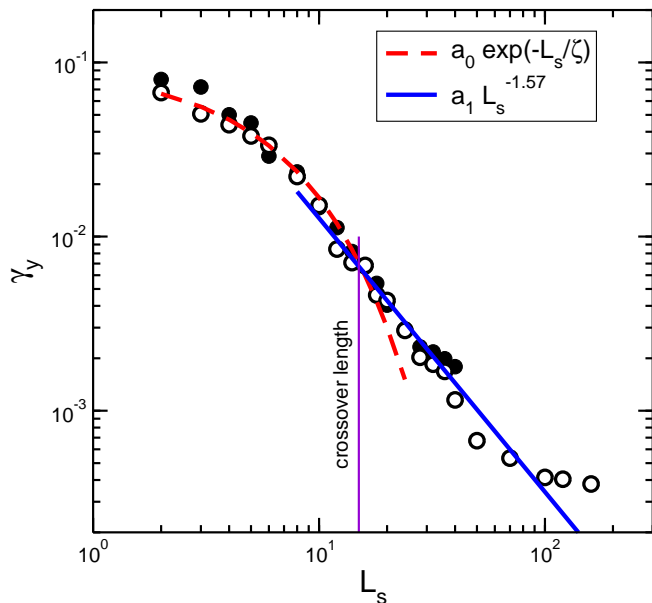


FIG. 4. **Large length scale behaviour.** Absolute yield strain  $\gamma_y$  as a function of subsystem size  $L_s$  for two different system sizes (opaque circle:  $L=90$  and open circle:  $L=320$ ) for the 2D BMLJ model (using poorly aged samples). Fit lines (red dashed line - exponential fit and solid blue line - power law fit with exponent 1.57) show a cross-over (at around 15a) from an exponential regime at small sub-systems to a power law regime at large sub-systems.

the functional form of the age dependence on  $\zeta$ .

## VI. LARGE LENGTH SCALE BEHAVIOUR - BEYOND $\zeta$ .

The macroscopic response of amorphous solids shows long-range elastic correlations [11] and power law avalanche statistics in the steady state [50]. Via numerical simulations done using periodic boundary conditions, it has been shown that, in the steady state, the finite size dependence of the average strain interval between two stress drops has the following behaviour:  $\langle \Delta\gamma \rangle \sim N^{-\beta} = L^{-\beta d}$ , where  $d$  is the dimension, and the exponent  $\beta \simeq 0.7$  [50]. One would thus expect that in 2D, the average strain interval for the first plastic drop should go as  $\langle \gamma_y \rangle \sim L^{-1.4}$ . We test whether this behaviour can be recovered at large sizes of the sub-box, for which we have utilized large system size soft matrix simulations ( $N = 125K$ ;  $L = 360$ ) and obtained average yield strain as a function of  $L_s$ . In Fig.4, we show the yield strain variation with changing  $L_s$  for the 2D BMLJ model (in a poorly aged sample) using two different system sizes ( $L = 90$  and  $L = 320$ ). We observe two interesting features. Firstly, with the increase in  $L_s$ , the average yield strain,  $\gamma_y(L_s)$ , crosses over from an exponential behaviour to a power law dependence having an exponent around 1.57. The crossover length is around

10a. Secondly, we find that in the limit of  $L_s \rightarrow L/2$ ,  $\gamma_y$  deviates from power law and seems to saturate, which likely originates from the effects due to periodic boundary condition. These observations highlight effectiveness of our the proposed soft-matrix in not only extracting the inherent length scale associated with sheared amorphous solids but also reproducing the large length scale behaviour. The power law exponent from our fit is not very off from the expected value [50], but we note that the soft elastic confinement employed in our method is different from the standard periodic boundary condition. This might affect the power-law exponent, which is an interesting direction for future investigations. Also, finite size effects cannot be ruled out. One needs to be sufficiently far away from the cross-over length scale to suppress all the effects of the underlying length scale. Hence for well annealed samples, one should go to larger system sizes to extract the same power-law exponent. Further it has been recently pointed out [51] that the asymptotic power-law behaviour with an exponent close to  $\beta \simeq 0.7$  can only be obtained at system sizes much larger for well annealed (ultra stable) glasses than currently accessible via computer simulation. Further studies across various models in different dimensions might shed more light on this puzzle.

## VII. LOCAL MECHANICAL PROPERTIES

After extracting the characteristic length scale  $\zeta$  using the soft matrix method, we employ this approach to determine the local yield threshold and local elastic modulus  $\mu_i$ . The local yield threshold (X) is defined as  $X = \sigma_y^i - \sigma_0^i$ , where  $\sigma_y^i$  and  $\sigma_0^i$  are the yield stress and zero strain stress at the local region  $i$ , whose linear size is of the order of  $\zeta$ . The local storage modulus  $\mu_i$  is obtained from the slope of the local load curve.

In Fig.5(a), we show for the 3D Soft-Rep system (using  $N = 97556$ ,  $L = 42a$  and  $k = 100$ ), the probability distribution function  $P(X)$  (inset) and cumulative distribution function  $F(X)$  (main panel) obtained from soft matrix as well as frozen matrix method [58]. We find that the frozen matrix not only overestimates the yield threshold, which would be expected, but also the functional behaviour is different. The fit lines in Fig.5(a) correspond to Weibull distribution  $F(X) = 1 - \exp[-(X/s_1)^{s_2}]$  with scale parameter  $s_1$  being 1.9 (soft matrix) and 1.5 (frozen matrix). The shape parameter  $s_2$ , which is associated with the instantaneous yield rate [59, 60], varies by a factor of 3, with  $s_2 = 2.3$  (soft matrix) and  $s_2 = 6.2$  (frozen matrix). Examining the implications of these differences on the mesoscale modeling results (where  $P(X)$  is a key input) would be an interesting aspect to explore.

In the Fig.5(b), we show  $P(\mu)$ , the distribution of local storage modulus along with a Gaussian fit. Unlike the frozen matrix method, which perturbs the elasticity of the background drastically, the soft matrix method allows for having the background elasticity close to the

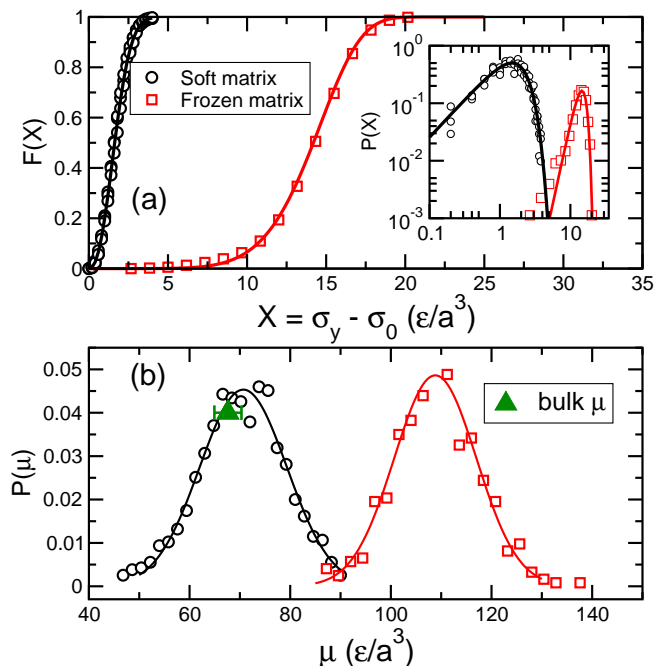


FIG. 5. **Local Mechanical Properties.** (a.) Distribution of local yield stress threshold ( $X = \sigma_y - \sigma_0$ ) for 3D soft-rep model (poorly aged), comparing the soft matrix (circle) with frozen matrix (square) methods. Inset shows the probability distribution  $P(X)$ , and the main figure show the cumulative distribution  $F(X)$ . The fit lines are drawn using Weibull distribution (see main text for details). (b.) Distribution of local shear modulus ( $\mu$ ) for 3D soft-rep model (poorly aged) comparing the two methods, shown along with Gaussian fits (using lines). Also marked is the bulk shear modulus (green triangle).

unconstrained bulk value and hence  $P(\mu)$  is distributed around the bulk value of the storage modulus (marked by green upper triangle in Fig.5(b)), which is measured from the slope of the load curve obtained from unconstrained simulations.

In conclusion, the soft matrix method introduced in this study not only enables the extraction of the length scale  $\zeta$ , but also provides improvements over the frozen matrix approach in terms of estimating local mechanical properties.

## VIII. SUMMARY AND DISCUSSION

We have devised a numerical technique for measuring local mechanical properties in amorphous solids. Labeled as the “soft matrix method”, we have utilized it to successfully extract the characteristic length scale associated with plastic events or non-affine displacements occurring during the deformation process. Our approach provides an opportunity to explore the local mechanical response within a purely elastic background. By applying this method to four different models of amorphous solids,

covering a wide range of materials, we have demonstrated the universal existence of this intrinsic length scale. Furthermore, we show that this length scale increases with the age of the sample, indicating its dependence on the preparation history. Importantly, our method allows us to accurately estimate the local yield threshold and local elastic modulus, greatly improving upon the accuracy of the existing frozen matrix method.

A natural question that arises from our results is the origin of the characteristic length scale,  $\zeta$ , in the material. The simplest interpretation is that  $\zeta$  corresponds to the spatial scale over which local plastic relaxations are devoid of any interfacial effects; i.e. it captures the intrinsic scale over which the first localized irreversible event would occur in a bulk system under mechanical loading. Thereby, it also relates to the spatial scale beyond which interference from other plastic events would come into play leading to screening of power-law correlations, as has been proposed recently [61]. Previous studies have extensively explored the concept of an intrinsic static correlation length scale associated with a putative amorphous order in supercooled liquids and glasses [15]. In the context of shear amorphous solids, similar length scales have been extracted using non-affine shear deformation protocols [28–31]. However, a comprehensive comparison with other measures of static length scale that do not involve shear deformation protocols, such as the point-to-set length scale [35], length scale derived from finite size scaling of relaxation times [36], and minimum eigenvalues [37], is currently lacking. It is expected that these different measures of static length scale in the supercooled liquid regime are proportional to each other [62].

Our work offers an opportunity to compare and investigate various length scales, shedding light on the origin of such correlations. The observed increase in  $\zeta$  with better annealing is consistent with the corresponding increase in the static correlation length obtained through analysis of non-affine displacement fields or finite size scaling of different observables in supercooled liquids. It also resembles the increase in the typical distance between soft spots as inferred from the measured number density of quasi-localized modes [63, 64]. However, without a detailed comparison, it is not immediately evident whether the length scale  $\zeta$  obtained using the soft matrix method is identical to these other length scales, although it is highly likely that  $\zeta$  is closely related to the length scale of quasi-localized modes. The connection to the static length scale of glass transition as determined by the point-to-set method is not apparent unless we assume that the point-to-set length scale and the length scale derived from finite size scaling of minimum eigenvalues are fundamentally the same [62].

Despite the aforementioned limitations, it is noteworthy that the characteristic length scale  $\zeta$  obtained through the soft matrix method exhibits remarkable similarity to the coarse-graining length scales reported in various studies on elasto-plastic models. These models often define an appropriate coarse-graining scale, typi-

cally around 5 in suitable units, to denote the size of elementary meso-block beyond which the propagation of plasticity occurs via the Eshelby kernel [40, 44–47, 49]. It is interesting to observe that in order to study the effect of ageing or annealing in these elasto-plastic models, systematically increasing the coarse-graining length scale is often required to achieve a comparable correspondence with microscopic simulations [51]. Hence, it appears that the length scale derived from the soft matrix method may serve as the desired length scale for the development of a robust mesoscopic elasto-plastic model capable of incorporating ageing or annealing effects in a more fundamental manner.

Overall, our work provides valuable insights into the behavior of amorphous solids at a local level, enhancing our understanding of their macroscopic properties and paving the way for improved mesoscale models required for material design.

## IX. METHODS

The four different models studied in this work are as follows.

(1.) **2D BMLJ:** Binary Mixture (65:35) of Lennard-Jones particles is a well-studied model glass forming system [65], whose mechanical properties are well characterised. Two different system size were considered,  $N=10K$  and  $125K$ , at a reduced density  $\rho = 1.2$ . The scales of A-A interactions within the model provide the units for length ( $a$ ), energy ( $\epsilon$ ).

(2.) **3D Soft-rep:** A system of 10% polydisperse soft spheres interacting via the WCA potential [66], is a typical colloidal model in 3D. At a volume fraction of  $\phi = 0.7$ , system size of  $N=1K, 5K, 10K$  and  $100K$  considered. the particle has an average diameter of  $a$  (unit length), mass  $m$  (unit mass), and energy  $\epsilon$  (unit mass).

(3.) **3D SiO<sub>2</sub>:** Most common molecular glass is modeled using the VSP modified BKS potential of 1:2 binary mixture of silicon and oxygen atoms [67]. System sizes of  $N = 13824, 46656$  particles at a density of  $\rho = 2.8 gm/cm^3$  are considered. In this model unit length is  $a_{Si-O}$ , unit energy  $\epsilon_{Si-O}$  and unit mass  $m_{Si}$ .

(4.) **3D Metallic Glass:** A metallic glass system  $Cu_{64.5}Zr_{35.5}$  alloy using the embedded atom model (EAM) [68]. System sizes  $N = 50000, 100000$  particles are considered at zero pressure. The units of length, mass, and energy are expressed in angstroms, grams/mole, and electron volts (eV), respectively. The lengths are scaled in terms of the diameter of Cu (2.56 angstroms).

### A. Sample preparation protocol

For 2D BMLJ and 3D Soft-rep systems, equilibrium NVT MD simulations were performed at  $T = 5.0 \epsilon/k_B$  with  $\rho = 1.2$  and  $\phi = 0.7$  respectively and equilibrated

configurations were quenched to  $T = 0.01$  at cooling rates  $\Gamma$  varying from  $10^{-2}$  to  $10^{-6}$ . These configurations were then subjected to potential energy minimization protocol (FIRE or Conjugate gradient, CG). For 3D Silica, configurations were equilibrated by NVT MD simulations at  $T \approx 3100 K$  and  $\rho = 2.8 gm/cm^3$  followed by instantaneous quench via potential energy minimization (CG). For 3D metallic glass, NPT MD simulations were performed at zero pressure and at temperatures  $T = 1100, 1200, 1300 K$  to equilibrate the system. Then configurations were quenched to  $T = 300K$  at cooling rates  $\Gamma = 10^{10}, 10^{11}, 10^{12} K/s$  followed by potential energy minimization by CG. In each model and cooling rate, a minimum of 10 to a maximum of 250 samples were prepared. The shear stress  $\sigma$  is computed from the off-diagonal term of the virial stress tensor, using the Irving-Kirkwood form [66].

### B. Shearing protocol

We probe the mechanical response using the Athermal Quasi-static Shear (AQS) protocol [69]. In this procedure, an elementary shear strain  $\delta\gamma \sim \mathcal{O}(10^{-5} - 10^{-6})$  is applied to a sample by the uniform affine deformation rule:  $x'_i = x_i + \delta\gamma y_i$ ,  $y'_i = y_i$ ,  $z'_i = z_i$  to all particles  $i$ . Following this step, the system is relaxed using an energy minimization technique (FIRE or CG). This sequence of deformation followed by minimization is thereafter continued. Here we chose the  $\delta\gamma$  such that in most of the samples we find only a single plastic event within the incremental strain window. The maximum applied strain  $\gamma_{max}$  was chosen such that at least one plastic event occurs within  $\gamma_{max}$ . In all our simulations, X is the shearing direction, Y is the gradient direction and Z is the vorticity direction.

### C. Plastic event or Yielding

To detect the plastic event or the yielding event, we measure the largest non-affine displacement in the system. The displacement is computed from two minimized configurations (separated by the elementary strain  $\delta\gamma$ ) and defined as  $\Delta z_{max}^2(\gamma) = \max[z_i(\gamma + \delta\gamma) - z_i(\gamma)]^2$  where  $z_i(\gamma)$  is the coordinate of a particle  $i$  in the direction perpendicular to shear (gradient direction in 2D and vorticity direction in 3D). By studying the corresponding drops in stress and the potential energy, we put a threshold on  $\Delta z_{max}^2$ , to identify the occurrence of the event;  $\Delta z_{max}^2$  is model dependent. We have also verified this identification via the back-shear protocol [46] and we find that our method provides an excellent balance between sensitivity of detection and computational efficiency. More details are provided in *SI*.

## ACKNOWLEDGEMENTS

PC, SK, SS and VVV acknowledge financial support from NSM grant DST/NSM/R&D\_HPC\_Applications/2021/29 as well as computational time on PARAM Yukti computing facility. SK acknowledges the Swarna Jayanti Fellowship,

grants DST/SJF/PSA01/2018-19, and SB/SFJ/2019-20/05. SS acknowledge the Faculty Initiation Grant from IIT Roorkee and PARAM Ganga computational facility. VVV acknowledge the computational time on the Chandra cluster at IIT Palakkad. Further we would like to thank Srikanth Sastry and Peter Sollich for fruitful discussions.

- 
- [1] D. Bonn, M. M. Denn, L. Berthier, T. Divoux, and S. Manneville, Yield stress materials in soft condensed matter, *Reviews of Modern Physics* **89**, 035005 (2017).
- [2] F. Varnik, L. Bocquet, and J.-L. Barrat, A study of the static yield stress in a binary lennard-jones glass, *The Journal of chemical physics* **120**, 2788 (2004).
- [3] C. A. Schuh, T. C. Hufnagel, and U. Ramamurty, Mechanical behavior of amorphous alloys, *Acta Materialia* **55**, 4067 (2007).
- [4] D. Rodney, A. Tanguy, and D. Vandembroucq, Modeling the mechanics of amorphous solids at different length scale and time scale, *Modelling and Simulation in Materials Science and Engineering* **19**, 083001 (2011).
- [5] J.-L. Barrat and A. Lemaitre, Heterogeneities in amorphous systems under shear, *Dynamical heterogeneities in glasses, colloids, and granular media* **150**, 264 (2011).
- [6] M. L. Falk and J. S. Langer, Deformation and failure of amorphous, solidlike materials, *Annu. Rev. Condens. Matter Phys.* **2**, 353 (2011).
- [7] S. M. Fielding, Shear banding in soft glassy materials, *Reports on Progress in Physics* **77**, 102601 (2014).
- [8] A. Nicolas, E. E. Ferrero, K. Martens, and J.-L. Barrat, Deformation and flow of amorphous solids: Insights from elastoplastic models, *Rev. Mod. Phys.* **90**, 045006 (2018).
- [9] A. Argon, Plastic deformation in metallic glasses, *Acta metallurgica* **27**, 47 (1979).
- [10] M. L. Falk and J. S. Langer, Dynamics of viscoplastic deformation in amorphous solids, *Physical Review E* **57**, 7192 (1998).
- [11] C. E. Maloney and A. Lemaitre, Amorphous systems in athermal, quasistatic shear, *Physical Review E* **74**, 016118 (2006).
- [12] J. D. Eshelby, The determination of the elastic field of an ellipsoidal inclusion, and related problems, *Proceedings of the royal society of London. Series A. Mathematical and physical sciences* **241**, 376 (1957).
- [13] A. Tanguy, F. Leonforte, and J. L. Barrat, Plastic response of a 2d lennard-jones amorphous solid: Detailed analysis of the local rearrangements at very slow strain rate, *The European Physical Journal E* **20**, 355 (2006).
- [14] K. Jensen, D. A. Weitz, and F. Spaepen, Local shear transformations in deformed and quiescent hard-sphere colloidal glasses, *Physical Review E* **90**, 042305 (2014).
- [15] S. Karmakar, C. Dasgupta, and S. Sastry, Length scales in glass-forming liquids and related systems: a review, *Reports on Progress in Physics* **79**, 016601 (2015).
- [16] P. K. Jaiswal, I. Procaccia, C. Rainone, and M. Singh, Mechanical yield in amorphous solids: A first-order phase transition, *Physical Review Letters* **116**, 085501 (2016).
- [17] G. P. Shrivastav, P. Chaudhuri, and J. Horbach, Yielding of glass under shear: A directed percolation transition precedes shear-band formation, *Physical Review E* **94**, 042605 (2016).
- [18] T. Divoux, M. A. Fardin, S. Manneville, and S. Lerouge, Shear banding of complex fluids, *Annual Review of Fluid Mechanics* **48**, 81 (2016).
- [19] M. Popović, T. W. de Geus, and M. Wyart, Elastoplastic description of sudden failure in athermal amorphous materials during quasistatic loading, *Physical Review E* **98**, 040901 (2018).
- [20] V. V. Vasisht, G. Roberts, and E. Del Gado, Emergence and persistence of flow inhomogeneities in the yielding and fluidization of dense soft solids, *Physical Review E* **102**, 010604 (2020).
- [21] M. Ozawa, L. Berthier, G. Biroli, A. Rosso, and G. Tarjus, Random critical point separates brittle and ductile yielding transitions in amorphous materials, *Proceedings of the National Academy of Sciences* **115**, 6656 (2018).
- [22] H. J. Barlow, J. O. Cochran, and S. M. Fielding, Ductile and brittle yielding in thermal and athermal amorphous materials, *Physical Review Letters* **125**, 168003 (2020).
- [23] P. Leishangthem, A. D. Parmar, and S. Sastry, The yielding transition in amorphous solids under oscillatory shear deformation, *Nature communications* **8**, 14653 (2017).
- [24] S. Sastry, Models for the yielding behavior of amorphous solids, *Physical Review Letters* **126**, 255501 (2021).
- [25] J. K. Dhont, A constitutive relation describing the shear-banding transition, *Physical Review E* **60**, 4534 (1999).
- [26] P. Schall and M. Van Hecke, Shear bands in matter with granularity, *Annual Review of Fluid Mechanics* **42**, 67 (2010).
- [27] V. V. Vasisht, M. L. Goff, K. Martens, and J.-L. Barrat, Permanent shear localization in dense disordered materials due to microscopic inertia, *arXiv preprint arXiv:1812.03948* **42** (2018).
- [28] E. R. Weeks, J. C. Crocker, and D. A. Weitz, Short- and long-range correlated motion observed in colloidal glasses and liquids, *Journal of Physics: Condensed Matter* **19**, 205131 (2007).
- [29] M. Mosayebi, E. Del Gado, P. Ilg, and H. C. Öttinger, Deformation of inherent structures to detect long-range correlations in supercooled liquids, *The Journal of Chemical Physics* **137**, 024504 (2012), <https://doi.org/10.1063/1.4732859>.
- [30] M. Mosayebi, P. Ilg, A. Widmer-Cooper, and E. Del Gado, Soft modes and nonaffine rearrangements in the inherent structures of supercooled liquids, *Phys. Rev. Lett.* **112**, 105503 (2014).
- [31] V. V. Vasisht, S. K. Dutta, E. Del Gado, and D. L. Blair, Rate dependence of elementary rearrangements and spa-



- tiotemporal correlations in the 3d flow of soft solids, *Physical review letters* **120**, 018001 (2018).
- [32] J. Goyon, A. Colin, G. Ovarlez, A. Ajdari, and L. Bocquet, Spatial cooperativity in soft glassy flows, *Nature* **454**, 84 (2008).
- [33] L. Bocquet, A. Colin, and A. Ajdari, Kinetic theory of plastic flow in soft glassy materials, *Physical review letters* **103**, 036001 (2009).
- [34] P. Jop, V. Mansard, P. Chaudhuri, L. Bocquet, and A. Colin, Microscale rheology of a soft glassy material close to yielding, *Physical review letters* **108**, 148301 (2012).
- [35] G. Biroli, J.-P. Bouchaud, A. Cavagna, T. S. Grigera, and P. Verrocchio, Thermodynamic signature of growing amorphous order in glass-forming liquids, *Nature Physics* **4**, 771 (2008).
- [36] S. Karmakar, C. Dasgupta, and S. Sastry, Growing length and time scales in glass-forming liquids, *PNAS* **106**, 3675 (2009).
- [37] S. Karmakar, E. Lerner, and I. Procaccia, Direct estimate of the static length-scale accompanying the glass transition, *Physica A: Statistical Mechanics and its Applications* **391**, 1001 (2012).
- [38] F. Spaepen, A microscopic mechanism for steady state inhomogeneous flow in metallic glasses, *Acta metallurgica* **25**, 407 (1977).
- [39] R. L. Jack, A. J. Dunleavy, and C. P. Royall, Information-theoretic measurements of coupling between structure and dynamics in glass formers, *Physical review letters* **113**, 095703 (2014).
- [40] M. Tsamados, A. Tanguy, C. Goldenberg, and J.-L. Barrat, Local elasticity map and plasticity in a model lennard-jones glass, *Phys. Rev. E* **80**, 026112 (2009).
- [41] J. Rottler, S. S. Schoenholz, and A. J. Liu, Predicting plasticity with soft vibrational modes: From dislocations to glasses, *Physical Review E* **89**, 042304 (2014).
- [42] P. Sollich, Lecture note, school on glass formers and glasses, bengaluru 2010 (2010).
- [43] H. Mizuno, S. Mossa, and J.-L. Barrat, Measuring spatial distribution of the local elastic modulus in glasses, *Phys. Rev. E* **87**, 042306 (2013).
- [44] F. Puosi, J. Olivier, and K. Martens, Probing relevant ingredients in mean-field approaches for the athermal rheology of yield stress materials, *Soft Matter* **11**, 7639 (2015).
- [45] S. Patinet, D. Vandembroucq, and M. L. Falk, Connecting local yield stresses with plastic activity in amorphous solids, *Physical review letters* **117**, 045501 (2016).
- [46] A. Barbot, M. Lerbinger, A. Hernandez-Garcia, R. García-García, M. L. Falk, D. Vandembroucq, and S. Patinet, Local yield stress statistics in model amorphous solids, *Physical Review E* **97**, 033001 (2018).
- [47] D. Richard, M. Ozawa, S. Patinet, E. Stanifer, B. Shang, S. A. Ridout, B. Xu, G. Zhang, P. K. Morse, J.-L. Barrat, L. Berthier, M. L. Falk, P. Guan, A. J. Liu, K. Martens, S. Sastry, D. Vandembroucq, E. Lerner, and M. L. Manning, Predicting plasticity in disordered solids from structural indicators, *Phys. Rev. Mater.* **4**, 113609 (2020).
- [48] V. V. Vasisht, P. Chaudhuri, and K. Martens, Residual stress in athermal soft disordered solids: insights from microscopic and mesoscale models, *Soft Matter* **18**, 6426 (2022).
- [49] C. Liu, S. Dutta, P. Chaudhuri, and K. Martens, Elastoplastic approach based on microscopic insights for the steady state and transient dynamics of sheared disordered solids, *Physical Review Letters* **126**, 138005 (2021).
- [50] S. Karmakar, E. Lerner, and I. Procaccia, Statistical physics of the yielding transition in amorphous solids, *Physical Review E* **82**, 055103 (2010).
- [51] E. Lerner, I. Procaccia, C. Rainone, and M. Singh, Protocol dependence of plasticity in ultrastable amorphous solids, *Physical Review E* **98**, 063001 (2018).
- [52] A. P. Thompson, H. M. Aktulga, R. Berger, D. S. Bolintineanu, W. M. Brown, P. S. Crozier, P. J. in 't Veld, A. Kohlmeyer, S. G. Moore, T. D. Nguyen, R. Shan, M. J. Stevens, J. Tranchida, C. Trott, and S. J. Plimpton, LAMMPS - a flexible simulation tool for particle-based materials modeling at the atomic, meso, and continuum scales, *Comp. Phys. Comm.* **271**, 108171 (2022).
- [53] R. L. Moorcroft, M. E. Cates, and S. M. Fielding, Age-dependent transient shear banding in soft glasses, *Physical review letters* **106**, 055502 (2011).
- [54] G. P. Shrivastav, P. Chaudhuri, and J. Horbach, Heterogeneous dynamics during yielding of glasses: Effect of aging, *Journal of Rheology* **60**, 835 (2016).
- [55] H. Bhaumik, G. Foffi, and S. Sastry, The role of annealing in determining the yielding behavior of glasses under cyclic shear deformation, *Proceedings of the National Academy of Sciences* **118** (2021).
- [56] D. Richard, E. Lerner, and E. Bouchbinder, Brittle-to-ductile transitions in glasses: Roles of soft defects and loading geometry, *MRS Bulletin* **46**, 902 (2021).
- [57] Around 250 samples were prepared at infinite to finite but higher  $\Gamma$ , 100 samples at moderate  $\Gamma$ , and 50 samples at the lowest  $\Gamma$ .
- [58] We find that in 2D systems, the fluctuations dominate the local load curve and hence noisy for  $N = 10K$ . Such issues are minimized when we study 3D systems.
- [59] R. Jiang and D. Murthy, A study of weibull shape parameter: Properties and significance, *Reliability Engineering & System Safety* **96**, 1619 (2011).
- [60] D. Ruan, S. Patinet, and M. L. Falk, Predicting plastic events and quantifying the local yield surface in 3d model glasses, *Journal of the Mechanics and Physics of Solids* **158**, 104671 (2022).
- [61] A. Lemaitre, C. Mondal, M. Moshe, I. Procaccia, S. Roy, and K. Sreiber-Re'em, Anomalous elasticity and plastic screening in amorphous solids, *Physical Review E* **104**, 024904 (2021).
- [62] G. Biroli, S. Karmakar, and I. Procaccia, Comparison of static length scales characterizing the glass transition, *Physical review letters* **111**, 165701 (2013).
- [63] D. Richard, G. Kapteijns, J. A. Giannini, M. L. Manning, and E. Lerner, Simple and broadly applicable definition of shear transformation zones, *Physical Review Letters* **126**, 015501 (2021).
- [64] D. Richard, G. Kapteijns, and E. Lerner, Detecting low-energy quasilocated excitations in computer glasses, *arXiv preprint arXiv:2303.12887* (2023).
- [65] R. Brüning, D. A. St-Onge, S. Patterson, and W. Kob, Glass transitions in one-, two-, three-, and four-dimensional binary lennard-jones systems, *Journal of Physics: Condensed Matter* **21**, 035117 (2008).
- [66] V. V. Vasisht and E. Del Gado, Computational study of transient shear banding in soft jammed solids, *Physical Review E* **102**, 012603 (2020).
- [67] I. Saika-Voivod, F. Sciortino, and P. H. Poole, Free energy and configurational entropy of liquid sil-

- ica: Fragile-to-strong crossover and polyamorphism, Phys. Rev. E **69**, 041503 (2004).
- [68] M. Mendeleev, Y. Sun, F. Zhang, C.-Z. Wang, and K.-M. Ho, Development of a semi-empirical potential suitable for molecular dynamics simulation of vitrification in cu-zr alloys, The Journal of Chemical Physics **151**, 214502 (2019).
- [69] C. E. Maloney and A. Lemaître, Amorphous systems in athermal, quasistatic shear, Phys. Rev. E **74**, 016118 (2006).

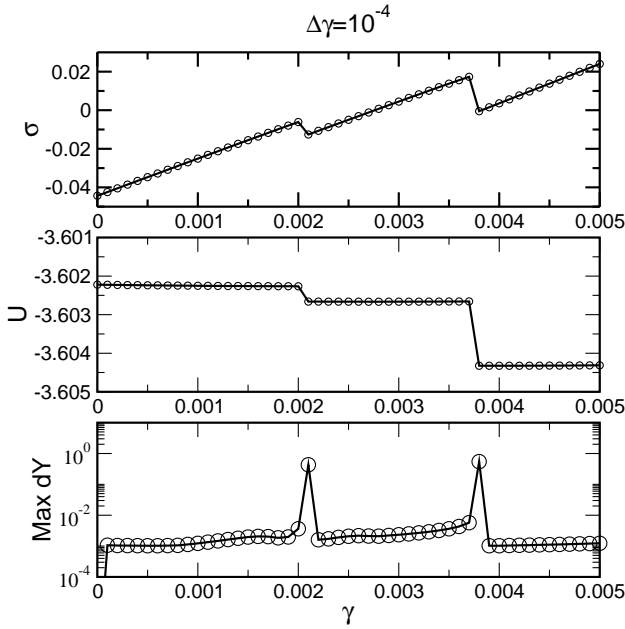


FIG. 6. **Evolution with strain** Stress  $\sigma$  and potential energy  $U$  evolve with applied strain. Jumps in these quantities observed as the system show local yielding due to plastic events, hence non-affine displacement captured by maximum displacement measure. This data is for 2D BMLJ model and poorly aged sample

SUPPLEMENTARY INFORMATION

Detecting plastic events

In Fig. 6 we show the evolution of the system’s shear stress ( $\sigma$ ), potential energy ( $U$ ) as well as the Maximum displacement with applied strain  $\gamma$ , for 2D BMLJ. Here we have considered the displacement in  $Y$  since the shearing direction is along  $X$ . In 3D systems, we consider  $Z$ , the vorticity direction. Clearly the jumps in the  $\sigma$  and  $U$  is signed in term of kinks in the displacement. In order to differentiate the signal from the background noise, we compute the distribution of these displacements and is shown in Fig. 7. It is quite evident that we have a bimodal distribution and we take conservative estimate for the threshold to recognize the plastic event as 0.01. This threshold is robust for varying ages of the sample. We carry out this analysis for other models to obtain the appropriate thresholds.

**Plastic events in subsystem with elastic background :** We perform the above analysis in the soft matrix as well wherein only a subsystem is allowed to have plastic events. Even though the bimodality of the displacement distribution is coarsened (see Fig. 8), the threshold for the plastic event is quite evident and recognize the events accurately (see Fig. 9).

Choice of  $k$  value in soft matrix

In the soft matrix method we allow the sub-system to relax completely without any constraint and the background is allowed relax affinely. This is achieved by addition of a spring potential with a spring constant  $k$ . The choice of  $k$  is made such that (1.) no large displacement occur in the background but also (2.) do not alter the system’s mechanical properties. In the Fig. 10 we show (for 2D BMLJ) the maximum displacement measured in the subsystem (left) and the full system (right), including the subsystem. For  $k=2$  and  $k=5$ , we find that relative large displacement are occurring in the surround and not in the subsystem. But with the increase the  $k$ , these events in the surrounding are curbed. In the Fig. 11 we show curvature of the PE profile (vs.  $\gamma$ ) before the plastic event, the storage module (from the slope of  $\sigma$  vs  $\gamma$  before the plastic event) as well as the pressure difference  $\Delta P = P_k - P_{k=0}$  for varying  $k$  values. These quantities are computed for the full system with soft matrix background. We find that for a range of  $k$  values ( $k_i=20$ ), these measures do change and are similar to bulk value (dashed line in Fig. 11). Hence  $k = 10$  is a good estimate which satisfy both the criterion defined above. Similar protocols are followed for other models.

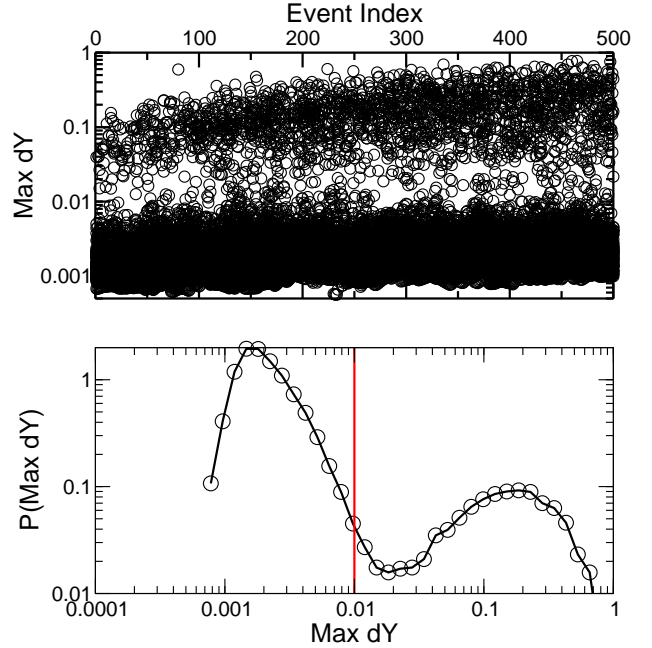


FIG. 7. **Maximum displacement distribution** Top plot show the raw data of maximum displacement and bottom its distribution. This data is for 2D BMLJ model and poorly aged sample

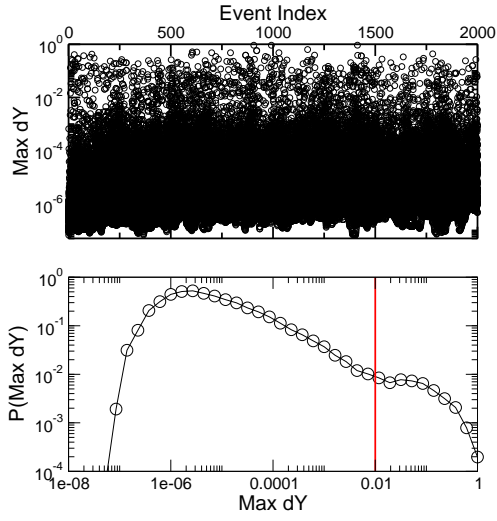


FIG. 8. **Maximum displacement distribution in soft matrix** Top plot show the raw data of maximum displacement and bottom its distribution, within the subsystem. This data is for 2D BMLJ model and poorly aged sample with a subsystem size of  $L_s = 16$ .

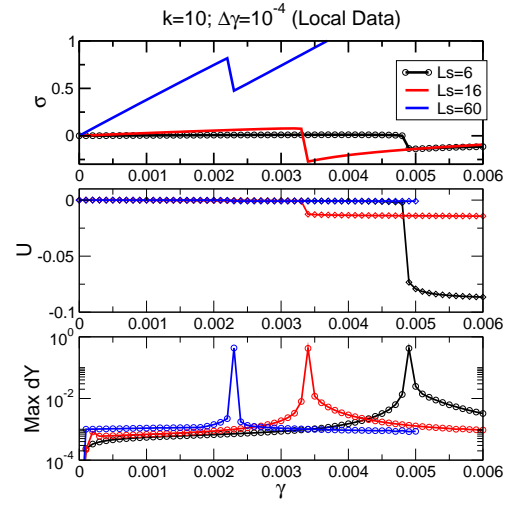


FIG. 9. **Evolution with strain in the subsystem** Stress  $\sigma$  and potential energy  $U$  evolve with applied strain. Jumps in these quantities observed as the system show local yielding due to plastic events in the sub-system. This data is for 2D BMLJ model (poorly aged) in a soft matrix of  $k=10$  and  $L_s = 16$ .

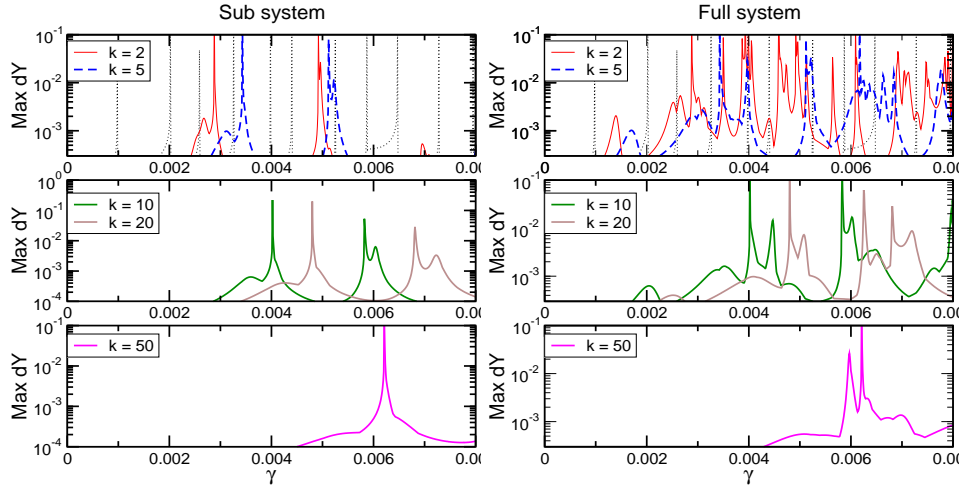


FIG. 10.  **$k$  dependence on events inside and outside the sub-system** Maximum displacement measure discussed in the text is computed for various  $k$  values, in the subsystem (left) and the full system (right) as a function of strain. The plastic event is signalled by the jump in the measure. Increasing the value of  $k$ , events occur only within the subsystem. This is for the 2D BMLJ system.

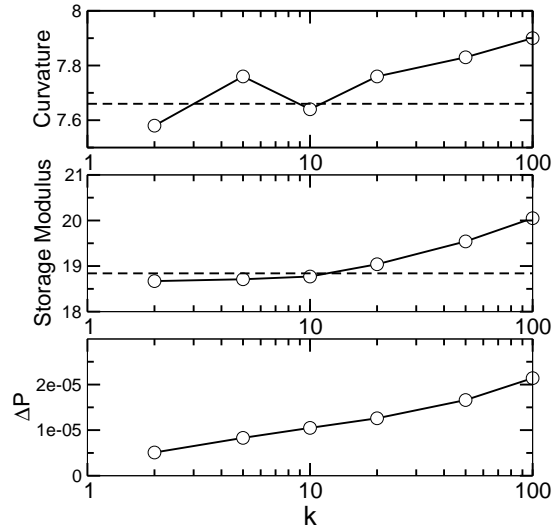


FIG. 11. **Various measures of the full system with a soft matrix background (2D BMLJ)** For  $k \leq 20$ , these measures do not vary substantially. The dotted line is the measure for unconstrained (without soft matrix) full system. Here  $\Delta P = P_k - P_{k=0}$  and is measure at small strain of  $10\delta\gamma$